UNEC Journal of Engineering and Applied Sciences **SECTION:**
Vol. 6, No.1, 2026, pp. 59-70 **ENGINEERING**
DOI: **https://doi.org/10.61640/ujeas.2026.0505** **SCIENCES**

Effects of nonlinear foundations on the nonlinear vibration behavior of multilayer heterogeneous cylindrical shells

A.H. Sofiyev[1,2,3*], T. Vergül[4]

[1]Department of Mathematics, Istanbul Ticaret University, Beyoglu, Istanbul 34445, Türkiye
[2]Scientific Research Department, Azerbaijan University of Architecture and Construction, Baku AZ1073, Azerbaijan
[3]Scientific Research Centers of Odlar Yurdu University Azerbaijan, Baku AZ1012 Azerbaijan
[4]Department of Civil Engineering, Istanbul Ticaret University, Beyoglu, Istanbul 34445, Türkiye
email: *aavey@ticaret.edu.tr*

Abstract

This study investigates the nonlinear vibration analysis of heterogeneous isotropic (HTI) layered cylindrical shells resting on a Winkler–Pasternak nonlinear elastic basis. The modulus of elasticity and density of the materials forming the HTI layer vary continuously, either together or separately, depending on the dimensionless thickness coordinate. The fundamental relationships are derived using von Kármán geometric nonlinearity and transverse shear deformation. Stress-deformation relationships for each HTI layer are formulated according to generalized Hooke's law, and then the fundamental equations are derived using these relationships. The fundamental differential equations are reduced to a time-dependent ordinary nonlinear differential equation using the Galerkin method. The exact solution is obtained in terms of Jacobian elliptic functions by solving the nonlinear differential equation under specific initial conditions. The responses of these parameters to nonlinear frequency are analyzed in detail by examining variations in basic rigidity, shear effects, heterogeneity, layer configuration, and geometric parameters.

***Keywords*:** Laminated shells, heterogeneity, nonlinear foundations, shear deformations, lay-up, nonlinear frequencies.

PACS numbers: 46.70.Hg,46.40.Ff, 05.45.-a

Received:	*Revised:*	*Accepted:*	*Published:*
11 November 2025	*15 January 2026*	*14 May 2026*	*31 May 2026*

1. Introduction

Structural elements composed of heterogeneous materials are frequently used in all areas of contemporary technology. Manufacturing and environmental influences such as radiation, temperature gradients, humidity, chemical agents, and mechanical processes alter material properties throughout the thickness, disrupting homogeneity while maintaining isotropy. The heterogeneity of materials necessitates more precise mechanical modeling to ensure reliability in advanced structural systems. In recent years, heterogeneous isotropic (HTI) materials have begun to be used more frequently in various environments, such as high-performance composites. Since the gradations in the material properties of structural elements used in these environments significantly affect their performance, investigating the nonlinear behavior of HTI multilayer configurations under the effects of elastic basis is of critical importance. The modeling of heterogeneous cylindrical shells relies on the elasticity theory of heterogeneous

continuous media, which is not yet fully integrated [1–5]. The fundamental studies on cylindrical shells, which are still frequently used today, are based on the Kirchhoff–Love theory, which has proven insufficient for moderately-thick shells [6–8]. This has led to the development of first-order shear deformation theory and higher-order theories for shell structures [9].

Since multilayer cylindrical shells, used in many applications such as pipelines and missile systems, interact with an elastic medium, linear Winkler, Pasternak, and elastic half-space models are widely used to model their behavior on foundations with different properties [10–12]. Although real foundations often exhibit nonlinear behavior, linear models are preferred in practice due to the difficulties arising from modeling. Shen's pioneering work on nonlinear foundations [13] has paved the way for numerous studies in this area [14–20]. The study of Shen and Williams [21] is a new initiative for multilayer isotropic shells, followed by Tornabene and colleagues who continued this work with their GDQ-based advanced approaches [22, 23]. Additional research includes post-buckling of piezo-layered shells [24], metaheuristic-based nonlinear buckling analyses [25], analytical formulations for hybrid nanocomposite shells on nonlinear foundations [26] and nonlinear vibration of homogeneous and heterogeneous laminated cylindrical shells on nonlinear elastic foundations [27-29].

The literature review revealed that the nonlinear vibration of heterogeneous multilayer cylindrical shells on a three-parameter nonlinear basis has not been sufficiently investigated within the scope of shear deformation theory (SDT). This study fills this gap and provides important implications for aerospace, defense, pressure vessels, pipelines, and nuclear applications.

Section 2 outlines the kinematic and constitutive relations for multilayer HTI shells based on extended shear deformation theory. Section 3 derives the nonlinear governing equations for shells on a three-parameter nonlinear foundation. Section 4 develops an analytical frequency–amplitude formulation via the semi-inverse method. Section 5 validates the approach and provides parametric studies. The concluding section summarizes the key contributions.

2. Basic equations

As shown in figure 1, the structure is a multilayer cylindrical shell composed of heterogeneous isotropic layers resting on a three-parameter nonlinear elastic foundation. The shell has length l, radius r, and total thickness h, with each of the N layers having equal thickness $H = hN^{-1}$. Perfect interlayer bonding is assumed, ensuring displacement continuity and eliminating interlayer pressure, so the classical shell-theory assumptions remain valid. The layers are also considered to undergo no slip or separation and retain their elastic behavior [9]. The coordinate system Oxyz is placed at the left end of the shell; for even N, the mid-surface lies at the interface between the two central layers, whereas for odd N it coincides with the central layer.

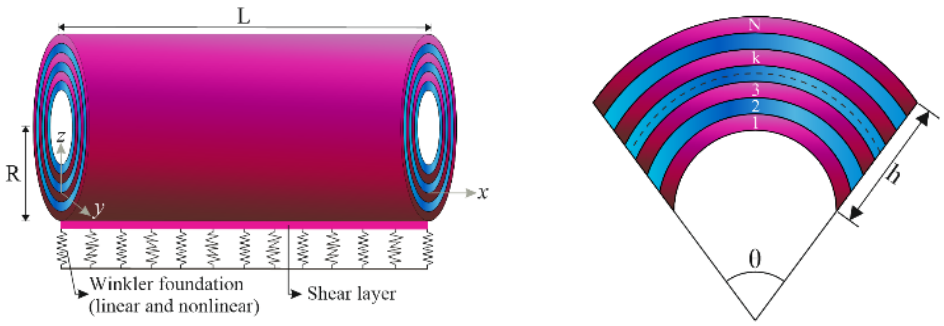

a) b)

Figure 1. Structural configuration of the multilayered cylindrical shell on a three-parameter nonlinear elastic foundation: a) overall geometry and b) cross-section

Schemes of one-, two-, three-, and four-layer configurations used in the numerical studies are shown in figure 2.

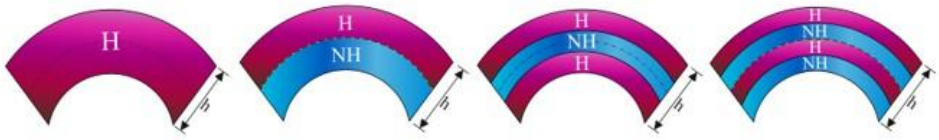

Figure 2. Sectional profile and material layering scheme of multilayered HTI cylindrical shells

The elastic modulus and density of each layer vary erexponentially through the dimensionless thickness coordinate $Z = z/h$ [3,15–17, 29]:

$$E^{(k)}(Z) = e^{\mu_1^{(k)}(0.5+Z)}\, E_0^{(k)}\,, G_{ij}^{(i)}(Z) = e^{\mu_1^{(k)}(0.5+Z)}\, G_{0ij}^{(k)}\ (i,j = 1,2,3, i \neq j),$$
$$\rho^{(k)} = e^{\mu_2^{(k)}(0.5+Z)}\, \rho_0^{(k)} \tag{1}$$

where $E_0^{(k)}$, $G_{0ij}^{(k)}$and $\rho_0^{(k)}$ denote the Young's modulus, shear modulus, and density of the homogeneous material in the *k*-th layer. The parameter $\mu_i^{(k)} \in [-1,1]$defines the degree of through-thickness variation, and $\mu_i^{(k)} = 0$represents a homogeneous isotropic layer.

Within the framework of the extended shear deformation theory, the complete set of governing nonlinear equations is derived for cylindrical shells constructed from HTI multilayers and supported by a nonlinear elastic foundation. These relations collectively describe the coupling between deformation modes, nonlinear elasticity, and foundation reactions, leading to the final nonlinear formulation expressed as:

$$h\big[(p_{11}-p_{31})\Phi_{,xxyy}+p_{12}\Phi_{,xxxx}\big]-p_{13}w_{,xxxx}-(p_{14}+p_{32})w_{,xxyy}+$$
$$+p_{15}\phi_{1,xxx}+p_{35}\phi_{1,xyy}-I_1\phi_{1,x}+(p_{18}+p_{38})\phi_{2,xxy}=0 \tag{2}$$

$$hp_{12}\Phi_{,yyyy}+h(p_{11}-p_{31})\Phi_{,xxyy}-(p_{32}+p_{14})w_{,xxyy}-p_{13}w_{,yyyy}+$$
$$+(p_{25}+p_{35})\phi_{1,xyy}+p_{38}\phi_{2,xxy}+p_{28}\phi_{2,yyy}-I_2\phi_{2,y}=0 \tag{3}$$

$$\frac{h\Phi_{,xx}}{r}-K_Lw-K_{NL}w^3+K_P\big(w_{,xx}+w_{,yy}\big)-\bar{\rho}w_{,tt}+I_1\phi_{1,x}+I_2\phi_{2,y}+$$
$$+h\big[\Phi_{,yy}\,w_{,xx}-2\Phi_{,xy}\,w_{,xy}+\Phi_{,xx}\,w_{,yy}\big]=0 \tag{4}$$

$$h\big[s_{11}\Phi_{,yyyy}+(2s_{12}+s_{31})\Phi_{,xxyy}+s_{11}\Phi_{,xxxx}\big]-s_{14}w_{,xxxx}-(2s_{13}-s_{32})w_{,xxyy}-$$
$$-s_{14}w_{,yyyy}+\frac{w_{,xx}}{r}+s_{25}\phi_{1,xxx}+(s_{15}+s_{35})\phi_{1,xyy}+(s_{28}+s_{38})\phi_{2,xxy}+$$
$$+s_{18}\phi_{2,yyy}-\big(w_{,xy}\big)^2+w_{,xx}\,w_{,yy}=0 \tag{5}$$

where $p_{ij}, s_{ij}(i,j = 1,2,3,4)$ and I_j are characteristic quantities that depend on both the heterogeneous material properties and the geometric configuration of the cylindrical shell and are defined in [28, 29], Φ is the Airy stress function , w is the deflection, $\phi_i, (i = 1,2)$ represent arbitrary functions that varies with the in-plane coordinates x and y, respectively, $\bar{\rho} = \sum_{k=1}^{N}\int_{z_{k-1}}^{z_k}\rho_0^{(k)}\, e^{\mu_2^{(k)}(0.5+Z)}\, dz$ is the inertia factor, in which $z_{k-1} = -0.5h + (k-1)hN^{-1}$, $z_k = -0.5h + khN^{-1}$, t is time,K_L (in N/m^3) is the linear Winkler coefficient, K_{NL} (in N/m^5) is the nonlinear spring coefficient, and it defines the increase or decrease in soil stiffness at large displacements (e.g., elastomeric foundations), K_P is the shear modulus of the Pasternak foundation.

3. Solution method

For multilayered HTI cylindrical shells supported by a nonlinear elastic foundation, the overall system of governing equations attains completeness only when accompanied by the appropriate boundary constraints. In the case of a simply supported shell, these constraints enforce compatibility between the displacement field and the admissible edge conditions, ensuring that both kinematic and static requirements are satisfied. Accordingly, the governing equations are supplemented by the following boundary conditions, which correspond to the classical simply supported configuration [9, 27]:

$$w = 0, M_{11} = 0, \varphi_2 = 0 \text{ as } x = 0, x = L \tag{6}$$

The solution to equations (2)-(5) is assumed in a prescribed analytical form that satisfies the geometric characteristics of the shell and is compatible with the imposed boundary conditions. Accordingly, the displacement field is represented through the following expression, which serves as the basis for constructing the nonlinear vibration formulation [28]:

$$w = w_1(t)\, sin(\lambda_1 x)\, sin(\lambda_2 y), \phi_1 = \phi_{11}(t)\, cos(\lambda_1 x)\, sin(\lambda_2 y), \\ \phi_2 = \phi_{22}(t)\, sin(\lambda_1 x)\, cos(\lambda_2 y) \tag{7}$$

where $w_1(t), \phi_{11}(t)$ and $\phi_{22}(t)$ are the unknown functions varying with time, whereas $\lambda_1 = \frac{m\pi}{l}, \lambda_2 = \frac{n}{r}$ are parameters associated with the axial and circumferential wave numbers, and (m, n) mode pairs represent the circumferential and axial mode numbers, respectively.

The Airy stress function is derived by inserting the assumed approximate functions given in equation (7) into the differential equation (5) and extracting the corresponding particular solution. This substitution leads directly to the following explicit form of the Airy stress function:

$$\Phi = \Gamma_1(t)\, cos(2\lambda_1 x) + \Gamma_2(t)\, cos(2\lambda_2 y) + \Gamma_3(t)\, sin(\lambda_1 x)\, sin(\lambda_2 y) \tag{8}$$

where

$$\Gamma_1(t) = \frac{q_{14} w_1^2(t)}{32 {\lambda_1}^4 q_3}, \Gamma_2(t) = \frac{q_{14} w_1^2(t)}{32 {\lambda_2}^4 q_1}, \Gamma_3(t) = \frac{q_{11} w_1(t) + q_{12}\phi_{11}(t) + q_{13}\phi_{22}(t)}{q_1 {\lambda_2}^4 + q_2 {\lambda_1}^2 {\lambda_2}^2 + q_3 {\lambda_1}^4}, \\ q_1 = s_{11}h, q_2 = (2s_{12} + s_{31})h, q_3 = s_{22}h, \\ q_{11} = {\lambda_1}^2\left[s_{14}\left({\lambda_1}^2 + {\lambda_2}^4\right) + (2s_{13} - s_{32}){\lambda_2}^2\right] + \frac{{\lambda_1}^2}{r}, \\ q_{12} = -\lambda_1\left[s_{25}{\lambda_1}^2 + (s_{15} + s_{35}){\lambda_2}^2\right], q_{13} = -(s_{28} + s_{38}){\lambda_1}^2\lambda_2 - s_{18}{\lambda_2}^3, q_{14} = {\lambda_1}^2{\lambda_2}^2 \tag{9}$$

By substituting the approximate expressions in equations (7) and (8) into the governing relations (2) – (4), and subsequently applying the Galerkin procedure to the resulting system, the auxiliary functions $\phi_{11}(t)$ and $\phi_{22}(t)$ appearing in obtaining equations are systematically removed. This reduction yields the final nonlinear equation of motion formulated within the framework of the extended shear deformation theory (EST) for multilayered HTI cylindrical shells supported by a nonlinear elastic foundation. The resulting nonlinear governing equation can thus be expressed as follows:

$$w_{,1tt} + \left(\Omega_{est}^{lwp}\right)^2 w_1(t) + \alpha_{nlest}^{nlw} w_1^3(t) = 0 \tag{10}$$

where, Ω_{est}^{lwp} is the linear natural frequency of multilayered HTI cylindrical shells on a two-parameter elastic foundation, and defined as follows:

$$\Omega_{est}^{lwp} = \sqrt{\frac{\bar{Y}_{31est}^{wp}}{\bar{\rho}}}, \alpha_{nlest}^{nlw} = \frac{Y_{32}}{\bar{\rho}}. \tag{11}$$

in which

$$\bar{Y}_{31est}^{wp} = \frac{1}{Y_{23}}\left[Y_{31est}^{wp}Y_{23} - Y_{34}Y_{21} + \frac{(Y_{33}Y_{23}-Y_{34}Y_{22})(Y_{11}Y_{23}-Y_{21}Y_{13})}{Y_{22}Y_{13}-Y_{23}Y_{12}}\right] \tag{12}$$

where $Y_{ij}(i,j = 1,2,3,4)$ are defined in [29].

In the framework of the EST, the nondimensional linear frequency parameter associated with multilayered HTI cylindrical shells resting on a Pasternak-type elastic foundation is determined through the following formulation:

$$\Omega_{1est}^{lwp} = \Omega_{est}^{lwp} r \sqrt{\{1 - [\nu^{(k)}]^2\}\frac{\rho_0^{(k)}}{E_0^{(k)}}} \tag{13}$$

To obtain a solution of the nonlinear ordinary differential equation presented in equation (10), the analysis employs the initial conditions stipulated as follows:

$$w_1(0) = A \text{ and } \quad \bar{w}_{,t}(0) = 0 \tag{14}$$

where $A = w_{max}$is the nondimensional amplitude.

To find the exact solution in terms of the Jacobi elliptic function, we transform (10) into the Jacobi elliptic function form. To do this, let's look for the solution as follows [6, 30]:

$$w_1(t) = A \cdot cn(\Omega t, k) \tag{15}$$

where $cn(\cdot, k)$ is the Jacobi elliptic cosine function, Ω is the effective angular frequency depending on the amplitude and the elliptic modulus (parameter).

As is known, the function $y(t) = cn(\Omega t, k)$satisfies the following nonlinear differential equation:

$$y_{,tt} + \Omega^2(1 - 2k^2)y + 2\Omega^2 k^2 y^3 = 0 \tag{16}$$

Since $w(t) = A\, cn(\Omega t, k)$and $w_{,1tt} = Ay_{,tt}$, the equation (16) takes the following form:

$$w_{1,tt} + \Omega^2(1 - 2k^2)w_1 + 2\Omega^2\frac{k^2}{A^2}w_1^3 = 0 \tag{17}$$

As the (17) is compared with the (10), the coefficients yield the following equality:

$$\Omega_{est}^{lwp} = \Omega\sqrt{1 - 2k^2}, \alpha_{nlest}^{nlw} = 2\Omega^2\frac{k^2}{A^2} \tag{18}$$

Since the period of the Jacobi elliptic **cn** function is $4K(k)$, the period of vibration depending on the amplitude is obtained as follows:

$$T(A) = \frac{4K(k)}{\sqrt{k_1 + k_3A^2}} \tag{19}$$

where the complete elliptic integral of the first kind, $K(k)$, is expressed by the following double factorial series for the module k:

$$K(k) = \frac{\pi}{2}\sum_{n=0}^{\infty} \left[\frac{(2n-1)!!}{(2n)!!}\right]^2 k^{2n} \tag{20}$$

From the expression (19), we obtain the nonlinear frequency–amplitude relation for multilayered HTI cylindrical shells resting on a nonlinear elastic foundation within the framework of EST as follows:

$$\Omega_{nlest}^{nlwp} = \frac{2\pi}{T(A)} = \frac{\pi\sqrt{\left(\Omega_{est}^{lwp}\right)^2 + \alpha_{nlest}^{nlw} A^2}}{2K(k)} \tag{21}$$

On the basis of this expression, the dimensionless nonlinear frequency–amplitude relation can be formulated in the following form:

$$\Omega_{1nlest}^{nlwp} = \Omega_{nlest}^{nlwp} r \sqrt{\{1 - [\nu^{(k)}]^2\}\frac{\rho_0^{(k)}}{E_0^{(k)}}} \tag{22}$$

Upon imposing the conditions $K_{NL} = K_P = K_L = 0$in equation (28), the analytical formulations corresponding to the shell configuration in the absence of any elastic foundation are obtained. Furthermore, setting $K_P = K_L = 0$yields the amplitude-dependent nonlinear frequency for multilayered HTI cylindrical shells supported by a two-parameter (Pasternak-type) elastic foundation. When $K_P = 0$, the resulting expressions characterize the dynamic response of shells resting on a nonlinear Winkler foundation. Finally, the conditions $K_{NL} = K_p = 0$ lead to the specialized case of a linear Winkler foundation, for which the amplitude-dependent nonlinear frequency are derived in a simplified form consistent with the absence of shear-layer and nonlinear foundation effects.

4. Numerical analysis and discussions

This section is divided into two main components. First, a set of benchmark tests is provided to demonstrate the accuracy and robustness of the theoretical framework established in the previous sections. Second, a detailed parametric study—conducted within both KLT and EST formulations—examines the influence of nonlinear foundation stiffness, HTI material gradation, layer architecture, and the number of layers on the linear and large-amplitude vibration responses of multilayer cylindrical shells.

4.1. Verification studies

This subsection presents reference-based assessments of both linear and nonlinear free-vibration behavior for isotropic cylindrical shells resting on Pasternak-type foundations as well as in the absence of foundation support. The first verification case is summarized in Table 1, where the nondimensional frequency parameters predicted by the present shear deformation formulation for isotropic square plates on a Pasternak foundation are compared with those reported by Zhou et al. [31] and Wang et al. [32]. The parameters employed in the comparison follow the data set provided in Wang et al. [32], as outlined below: $b = 100h$, $l/b = 1$, $K_L = 100D_0^{(1)}$ and $K_P = 10D_0^{(1)}$. For the purpose of performing the numerical calculations,

$$k = 1, r \to \infty, n_1 = \frac{n\pi}{l}, \eta_i^{(k)} = 0$$

is assumed in expression (24). As in the studies Zhou et al. [31] and Wang et al. [32], the DNLFP is obtained using the relation

$\widehat{\omega}_{1lest}^{lwp} = \omega_{lest}^{lwp}\left(\frac{b}{\pi}\right)^2\sqrt{\frac{\rho_0^{(1)}h}{D_0^{(1)}}}$, where $D_0^{(1)} = \frac{E_0^{(1)}h^3}{12\left[1-\left(\nu_0^{(1)}\right)^2\right]}$. In the comparison, the following mechanical properties is used:

$$\eta_i^{(k)} = 0, E_0^{(k)} = 2.1\times10^{11}Pa, \nu_0^{(k)} = 0.3, \rho_0^{(k)} = 7850kg/m^3, k = 1.$$

Table 1 demonstrates that the results obtained through the present formulation closely align with the benchmark solutions reported in [31] and [32].

	$\hat{\omega}_{1lest}^{lwp}(m,n)$		
Zhou et al. [31]	2.6551 (1,1)	5.5717 (1,2)	5.5717 (2,1)
Wang et al. [32]	2.6551 (1,1)	5.5717 (1,2)	5.5717 (2,1)
Present study	2.6557 (1,1)	5.5761 (1,2)	5.5761 (2,1)

Table 1. Comparison of the $\widehat{\omega}_{1lest}^{lwp}$ for isotropic square elastic plates resting on a two-parameter linear elastic foundation

4.2. Nonlinear analysis

The study further explores how transverse shear effects, distinct patterns of material nonhomogeneity, alternative elastic foundation representations, and various multilayer arrangements influence the nondimensional nonlinear frequency response of cylindrical shells. Particular attention is given to the evolution of the nonlinear frequency as a function of the vibration amplitude A, with detailed trends presented and discussed. For clarity, the material models employed throughout the tables are denoted using the following abbreviations: The types of isotropic heterogeneous materials used in all tables and figures are defined as follows: if $\eta_1^{(k)} = \eta_2^{(k)} = 0$ material is homogeneous and is shown as H, if $\eta_1^{(k)} = 1, \eta_2^{(k)} = 0$ material is heterogeneous and is shown as NH_1, $\eta_1^{(k)} = 1, \eta_2^{(k)} = 1$ material is heterogeneous and is shown as NH_2, if $\eta_1^{(k)} = -1, \eta_2^{(k)} = 0$ material is heterogeneous and is shown as NH_3, if $\eta_1^{(k)} = -1, \eta_2^{(k)} = -1$ material is heterogeneous and is shown as NH_4 . Soil Type 1: $K_L = 0, K_{NL} = 9\times10^{14}, K_p = 0$; Soil Type 2: $K_L = 9\times10^{10}, K_{NL} = 9\times10^{14}, K_P = 0$; Soil Type 3: $K_L = 9\times10^{10}, K_{NL} = 9\times10^{14}, K_P = 9\times10^{6}$. In the homogeneous material properties and geometric parameter of the shell are taken as $E_0^{(k)} = 2.1\times10^{11}Pa, \nu_0^{(k)} = 0.3, \rho_0^{(k)} = 7850kg/m^3$ and $h = 0.01m, r = 20h, l = 0.25r$.

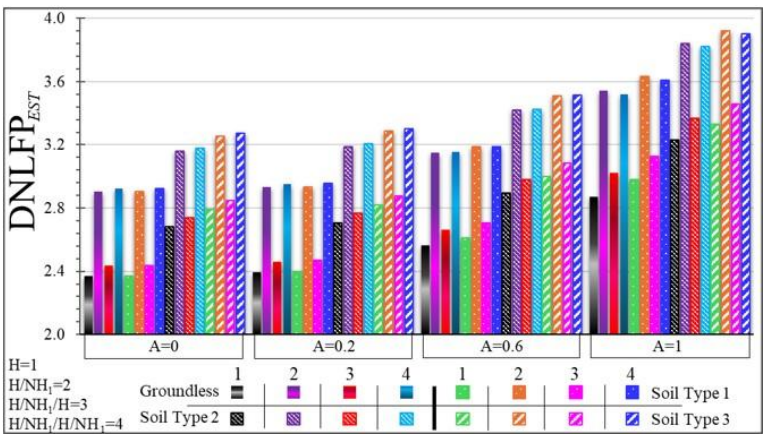

Figure 3. Variation of the DNLFP within EST for single-layer H, three layered cylindrical shells containing NH_1 layer with respect to A with different soil types

Figures 3–10 illustrate the evolution of the dimensionless nonlinear frequency parameter (DNLFP) with respect to the amplitude A for single-layer homogeneous shells, two-, three- and four-layer configurations incorporating HTI (i=1,2,3,4) layers, evaluated under both EST and KLT formulations for three type soil conditions. Across all configurations—homogeneous or heterogeneous, with or without foundation support—the DNLFP increases monotonically as the vibration amplitude grows. The circumferential wave number is set to one throughout the analysis.

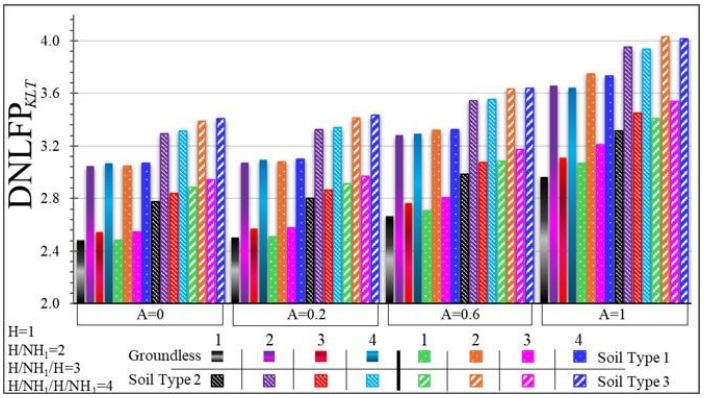

Figure 4. Variation of the DNLFP within KLT for single-layer H, three layered cylindrical shells containing NH_1 layer with respect to A with different soil types

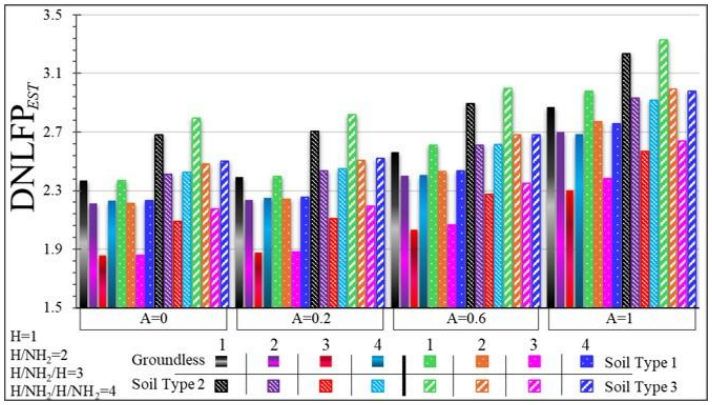

Figure 5. Variation of the DNLFP within EST for single-layer H, four-layered cylindrical shells containing NH_2 layer with respect to A with different soil types

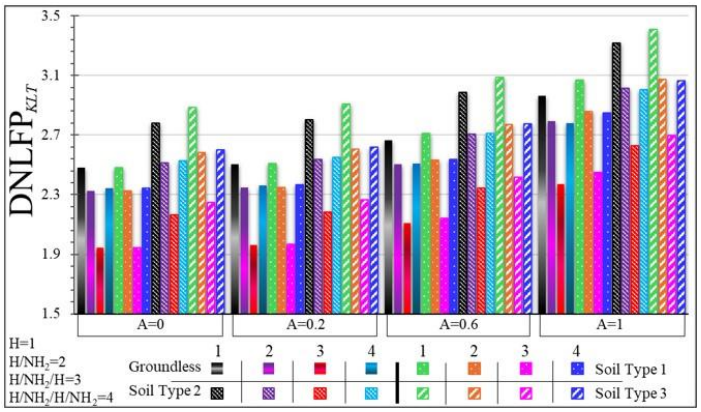

Figure 6. Variation of the DNLFP within KLT for single-layer H, four-layered cylindrical shells containing NH_2 layer with respect to A with different soil types

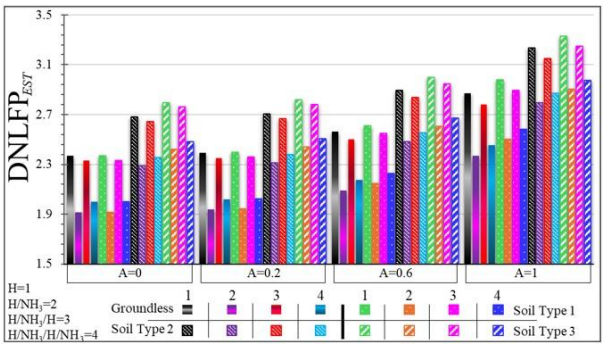

Figure 7. Variation of the DNLFP within EST for single-layer H, three-layered cylindrical shells covered by NH_3 layers layer with respect to *A* with different soil types

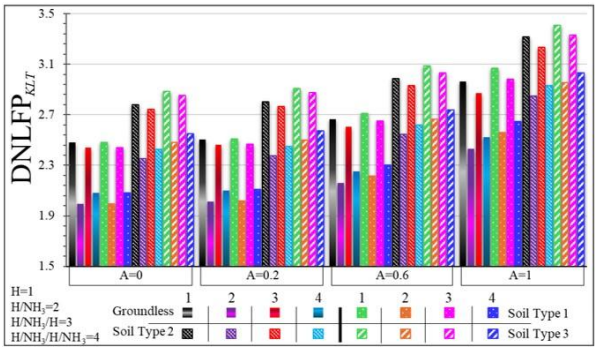

Figure 8. Variation of the DNLFP within KLT for single-layer H, three-layered cylindrical shells covered by NH_3 layers layer with respect to *A* with different soil types

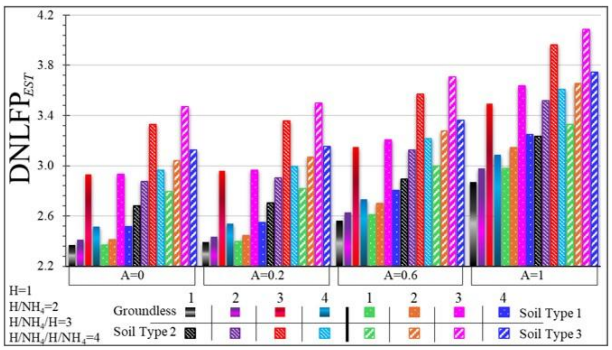

Figure 9. Variation of the DNLFP within EST for single-layer H, four-layered cylindrical shells covered by NH_4 layers layer with respect to *A* with different soil types

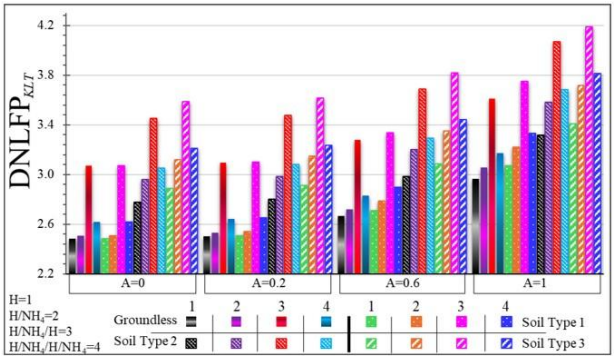

Figure 10. Variation of the DNLFP within KLT for single-layer H, four-layered cylindrical shells covered by NH_4 layers layer with respect to *A* with different soil types

In general, the effect of the HTI layer compared to the H layer in a soilless environment is highly sensitive to the location. The strongest improvement is observed in configurations where the NH layer is close to the outer surface, while the most negative effect is observed in configurations with NH layers located in the middle. In soil type 1, the improving or weakening effects of the NH layer compared to the H layer persist, but the soil stiffness partially offsets the effect of the NH layer. For instance, in NH layers near the outer surface (H/NH_1), the positive effect compared to the H layer remains dominant, but weakens slightly from 22.3% to 21.8% with increasing A (figures 3 and 4). In intermediate NH layers, the negative effect is largely maintained, but some improvements are observed (from -19% to -16.2% for H/NH_3) (see, figures 7 and 8). In NH layers near the inner surface (H/NH_4), the positive effect becomes stronger from 1.88% to 5.47% with increasing A (figures 9 and 10). This soil type moderates the effect of the NH position, but does not completely alter the fundamental positive/negative trend of NH on H. In soil type 2, the effect of NH contribution relative to H exhibits a more systematic and stable behavior compared to the no-soil case: NH layers near the outer surface clearly outperform H (from 19% to 18.8%). The negative effect persists in intermediate locations but becomes slightly less pronounced (from -14.6% to -13.5% for H/NH_3). Inner-located NH layers clearly increase their positive contribution relative to H (from 7.4% to 8.8% in H/NH_4). This soil type more significantly stabilizes the effects of the NH layer and strengthens the role of the NH contribution within the system. In soil type 3, because the soil is much stiffer, the effect of the NH layers relative to H becomes the most consistent and predictable. The NH layer near the outer surface again provides a strong increase relative to H (from 16.7% to 17.8%). The middle NH layers maintain the negative effect, but the difference decreases (from -13.4% to -12.7% in H/NH_3). The inner NH layers further increase the positive effect (for H/NH_4 from 9% to 9.8%). In four-layered arrangements, some effects remain constant (e.g., for $H/NH_1/H/NH_1$ is 17.3%) or change only slightly, indicating a stabilization of the NH effect at high stiffness.

When the effect of SD on the DNLFP is examined, it is seen that the SD-induced reductions weaken considerably as A increases from 0.2 to 1 in the groundless environment. Initially, the SD effect is around (–4%) to (–5%) for configurations containing H or NH layers near the outer surfaces (e.g., H, H/NH_1, H/NH_2, $H/NH_1/H$, $H/NH_1/H/NH_1$), while configurations with NH located more inward show slightly smaller around (–3%) to (–4%) reductions (figures 3-10). At A = 1, these values collectively decrease to approximately (–2.5%) to (–3.3%), indicating a consistent weakening of roughly 1–1.5 percentage points across all alignments. An increase in A regularly reduces the SD effect, regardless of the layer sequence. For soil type 1, within the SDT framework, reductions in A at small values cluster between approximately (-4%) and (-5%) for most homogeneous or outer heterogeneous layered shells, while in sequences containing HT in the middle, they are around (-3%) and (-4%). When A = 1, all effects cluster in a narrower range, approximately (-2.3%) to (-3.2%), indicating that it accelerates the weakening of the SD effect on frequency. In soil type 2, reductions start at lower levels, generally clustering between (-2.7%) and (-4%) depending on the location of HT in the layer, while as A increases, these values settle between (-1.9%) and (-2.9%). In soil type 3, the effects of the initial SD on frequency are between (-2.4%) and (-3.8%), and for A = 1, approximately (-1.7%) to (-2.8%).

In general, for all soil types and hybrid arrays, increasing the A parameter monotonically weakens the negative effect of SD on DNLFP; this improvement trend becomes stronger as the soil stiffness increases.

In the SDT framework, the soil effect on DNLFP increases in all configurations but shows different trends in each soil type as the A parameter increases from 0.2 to 1.This increase, for example, increases from 0.25% to 3.83% in the H configuration, while in hybrid configurations (H/NH_1, H/NH_3, $H/NH_1/H$, $H/NH_3/H$, etc.), the initially quite low levels (0.13%–0.37%) increase to 2.5%–5.5% at A =1. This indicates that soil type 1 provides additional but moderate stiffness to the system, and as A increases, the ground contribution becomes an increasingly

stronger component due to the increased effective resistance of the shell. The sharper increase in the ground effect, particularly in configurations with high NH content, indicates that material heterogeneity increases the sensitivity to the ground. In soil type 2, the ground effect tends to decrease slightly with increasing A. For example, while the value decreases from 13% to 12.6% in the H configuration, the decreases in the other configurations are similarly very limited (e.g., from 8.8% to 8.5% in H/NH_1, from 19.3% to 18.1% in H/NH_3). This trend indicates that soil type 2 adds more significant stiffness to the system, but with an increase in A, the internal stiffness of the shell becomes dominant, thus damping the ground effect relatively. The largely parallel decrease in the different configurations indicates that the configurational dependence of the structure-soil interaction in this type of configuration. In soil type 3, the ground effect is initially quite high (e.g., 17.7% in H configuration, 26% in H/NH_3) and decreases significantly in all configurations as A increases (15.9% and 22.7%, respectively). This large-scale weakening demonstrates that the third soil type provides the highest stiffness to the system, and that the shell behavior becomes increasingly independent of the soil effect as the A parameter increases. Thus, the soil contribution, while initially strong, ceases to be dominant as A increases, becoming a secondary influence. This is particularly evident in multilayered arrays (H/NH_1/H, H/NH_3/H/NH_3, etc.), confirming that soil stiffness is one of the key parameters controlling the stress-strain distribution in the nanocomposite structure (figures 3-10).

4. Conclusion

This study presents a nonlinear vibration analysis of multilayer HTI cylindrical shells resting on a nonlinear elastic foundation using Donnell-type theory with von Kármán geometric nonlinearity and transverse shear effects. The stress–displacement relations follow generalized Hooke's law, and the governing equations are derived accordingly. Through Galerkin method, the PDEs are transformed into second-order nonlinear ODEs, and exact solutions are obtained in terms of the Jacobian elliptic function. The numerical analyses can be summarized in the following four points: DNLFP increases as amplitude increases for all material distributions and foundation types, while the SD effect weakens, and this weakening is accelerated by the presence of soil; as soil rigidity increases, especially in high soil type 3, the effect of SD on DNLFP is largely suppressed, and the differences between layer arrangements become negligible; the effect of the NH layer on DNLFP is position-sensitive: it enhances at the outer surface, weakens in the middle region, and provides a moderately positive contribution at the inner surface; in multilayered structural elements, the effect of low-rigidity soil on DNLFP is more pronounced, while at high-rigidity, amplitude becomes the dominant parameter determining the system behavior. Overall, the study demonstrates that the nonlinear dynamic response of multilayer and heterogeneous cylindrical shells is governed not only by material gradation but also by soil–shell interaction and the accurate modeling of shear effects. These results provide a rigorous foundation for future optimization, material tailoring, and advanced numerical modeling of multilayer composite shells.

References

1. V.A. Lomakin, Theory of Elasticity of Inhomogeneous Bodies. Moscow University, Moscow (1976) 368p.
2. Y.M. Grigorenko, A. T. Vasilenko, and N. D. Pankratova, Elasticity Theory Problems for Heterogeneous Bodies [in Russian], Naukova Dumka, Kiev (1991).
3. A.H. Sofiyev, and E. Schnack, Acta Mech. **162**(1) (2003) 29.
4. J. Awrejcewicz, and V.A. Krysko, Springer, Berlin, Heidelberg (2008) 15.
5. H.S. Shen, Functionally Graded Materials: Nonlinear Analysis of Plates and Shells, CRC Press, Boca Raton, FL (2016) 280p.
6. A.S. Vol'mir, Nonlinear Dynamics of Plates and Shells [in Russian], Nauka, Moscow (1974) 544p.

7. W. Leissa, Vibration of Shells, NASA Scientific and Technical Information Office, Washington, DC (1973) 438p.
8. M. Amabili, Nonlinear Vibrations and Stability of Shells and Plates, Cambridge University Press (2010) 374p.
9. J. N. Reddy, Mechanics of Laminated Composite Plates and Shells: Theory and Analysis, CRC Press, New York (2004) 855p.
10. P.L. Pasternak, On a New Method of an Elastic Foundation by Means of Two Foundation Constants, Gosstroyizdat, Moscow (1954).
11. M. I. Gorbunov-Possadov, T. A. Malikova, and V. I. Solomin, Design of Structures on Elastic Foundation, Gos. Izd. Lit. Stroit. Arkh, Moscow (1984).
12. D. Younesian, A. Hosseinkhani, H. Askari, and E. Esmailzadeh, Nonlinear Dyn. **97**(1) (2019) 853.
13. H. S. Shen, Eng. Struct. **17**(6) (1995) 407.
14. Q. Qian, L. Wang, and Q. Ni, Acta Mech. Solida Sin. **21**(2) (2008) 170.
15. A.H. Sofiyev, Compos. Part B Eng. **98** (2016) 141.
16. H. Sofiyev, N. Kuruoglu, Compos. Struct. 166 (2017) 153.
17. H. Sofiyev, Z. Karaca, and Z. Zerin, Compos. Struct. **159** (2017) 53.
18. H. Ahmadi, Eng. Comput. **35**(4) (2019) 1491.
19. I. Zemlyanukhin, A. V. Bochkarev, V. I. Erofeev, and A. V. Ratushny, Wave Motion **114** (2022) 103020.
20. V.N.V. Hoang, P.T. Thanh, and L. Toledo, Ocean Eng. **307** (2024) 118123.
21. H. S. Shen, and F. W. Williams, Int. J. Non-Linear Mech. **30**(5) (1995) 651.
22. F. Tornabene, and J. N. Reddy, J. Indian Inst. Sci. **93**(4) (2013) 635.
23. F. Tornabene, N. Fantuzzi, M. Bacciocchi, and J. N. Reddy, Compos. B Eng. **126** (2017) 162.
24. K.M. Fard, and M. Bohlooly, Compos. Struct. **171** (2017) 360.
25. K. Foroutan, S. M. Varedi-Koulaei, N. D. Duc, and H. Ahmadi, Eur. J. Mech. A/Solids **91** (2022) 104420.
26. P. Zhang, Z. Meng, H. Wei, and N. Liu, J. Vib. Eng. Technol. **12** (2024) 77.
27. A.H. Sofiyev, and M. Avey, ZAMM **105** (2025) e70213.
28. H. Sofiyev, and T. Vergül, Thin-Walled Struct. **220** (2025) 114388.
29. H. Sofiyev, T. Vergül, and F. Kadıoğlu, J. Appl. Comput. Mech. (2025).
30. X. Wu, and X. Wang, Chaos Solitons Fractals 18(4) (2003) 721.
31. D. Zhou, Y. K. Cheung, S. H. Lo, and F. T. K. Au, Int. J. Numer. Meth. Eng. **59**(10) (2004) 1313.
32. Q. Wang, D. Shi, and X. Shi, Meccanica **51** (2016) 1985.